Bulletin of Geophysics and Oceanography Vol. 65, n. 2, pp. 149-164; June 2024
DOI 10.4430/bgo00429

How to model thick thermo-poro-elastic inclusions

C. Benussi, M.E. Belardinelli and M. Nespoli

Department of Physics and Astronomy Augusto Righi, University of Bologna, Bologna, Italy

(Received: 28 April 2023; accepted: 25 July 2023; published online: 29 September 2023)

ABSTRACT Volcanic regions can be characterised by different unrest phenomena and secondary volcanism. Several studies link these phenomena to both magma and hydrothermal fluids. For instance, in the case of the widely studied Campi Flegrei caldera, recent literature suggests that thermo-poro-elastic (TPE) inclusion models are suitable to describe both the observed deformation and seismicity that often accompany its unrest episodes. Some recent works propose analytical solutions to model the case of a thin disc-shaped inclusion, i.e. with a thickness much smaller than its radius. As this restriction may be critical, TPE inclusion models were subsequently extended to cylindrical-shaped inclusions, with an arbitrary thickness, by representing them as a superposition of several thin disc-shaped inclusions (elements). In this paper, we demonstrate how to estimate the minimum number of elements to represent both displacement and stress fields caused by cylindrical TPE inclusions with an arbitrary aspect-ratio (thickness over radius). For aspect ratios greater than 0.3, a single element model will no longer prove suitable to represent both displacement and stress with a good accuracy.

Key words: deformation source, thickness, TPE inclusion, thermo-poro-elasticity, discretisation.

1. Introduction

The study of deformation sources in volcanic and hydrothermal areas is a very interesting topic, which has been widely discussed in the past and in recent literature (e.g. Bonafede *et al*., 2022 and references therein). For example, Campi Flegrei is a restless caldera in a densely populated area, with a complex hydrothermal system, and a long historical activity record. The uplift and subsidence (bradyseism) phenomena have been known since the Roman period, for which variations between 1 to 10 m have been estimated. Significant uplift occurred between 1950 and 1985 (about 4 m). In the 1982-1984 period, the centre of the caldera was uplifted by 1.8 m (Belardinelli *et al*., 2011; Trasatti *et al*., 2011). At the same time, a series of earthquakes, with magnitudes up to M_L 4.2, was recorded. This episode was followed by about 1 m of subsidence between 1985 and 2000 (Del Gaudio *et al*., 2010). As shown in Fig. 1b, a new uplift phase started in 2005, and continues to this day.

Today, the Campi Flegrei caldera is characterised by an intense hydrothermal activity, which, as such, represents a suitable study area to understand and apply different deformation source models. The driving force behind the ground deformation at Campi Flegrei is still a matter of debate. So far, various models have been evaluated, including the intrusion of new magma and/or hydrothermal circulation (De Vivo *et al*., 2020). Recent literature agrees that ground deformation and seismicity are often connected to fumarole and hydrothermal activities (Chiodini *et al*., 2021).

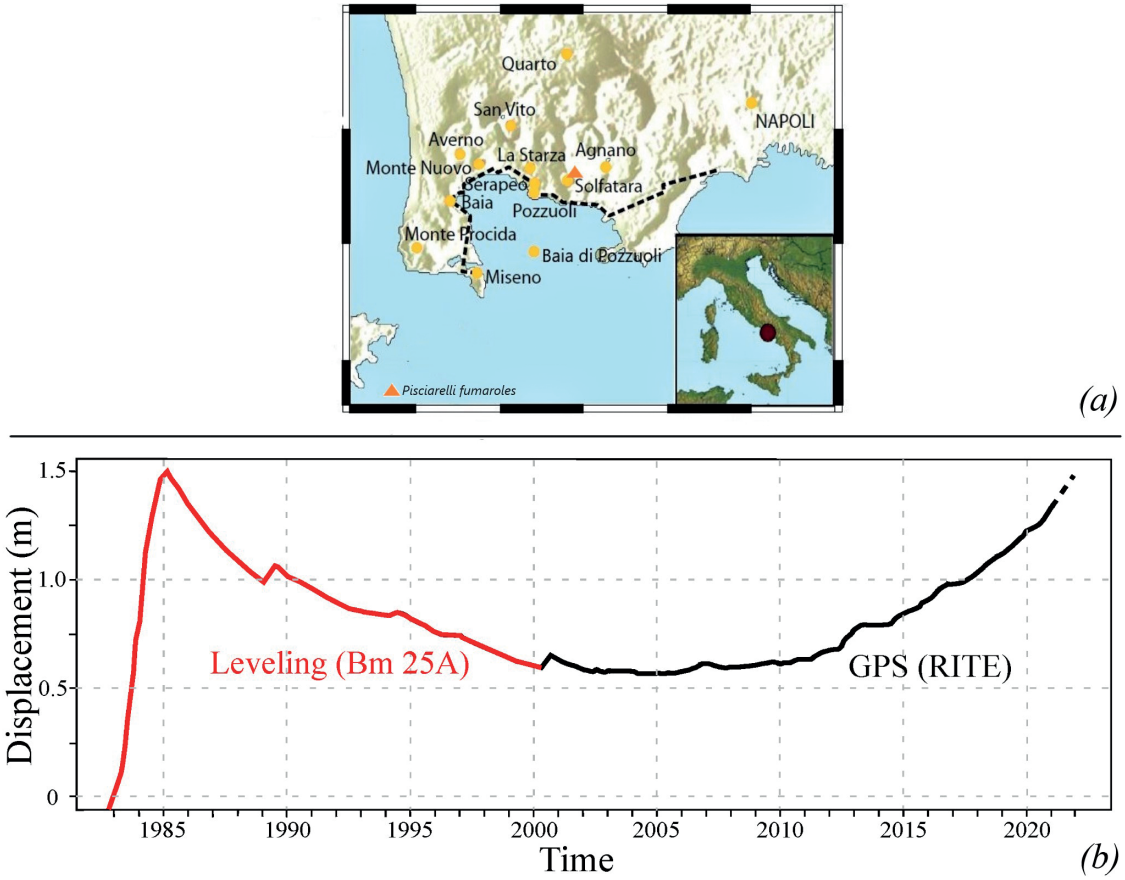

Fig. 1 - Map of the Campi Flegrei area, near Naples in Italy (a) and time series of vertical uplifts (b) measured with levelling at the benchmark 25A [red curve: Del Gaudio *et al*. (2010)] and at the CGPS RITE station [black curve: De Martino *et al*. (2021)]. Both the benchmark and RITE station are located in Pozzuoli.

The displacement, deformation and stress fields in volcanic and hydrothermal areas can be modelled using deformation sources under different assumptions. Some of the most used deformation sources are described by Mogi (1958), Yang *et al*. (1988), and Fialko *et al*. (2001). The first two models represent magma filled pressurised cavities, while the third is suitable to describe circular and horizontal cracks. Purely magmatic models do not explain long-term subsidence (Troise *et al*., 2018). Moreover, a null deviatoric stress is present inside this kind of source, thus preventing the occurrence of seismicity in the source interior. Furthermore, the presence of large magmatic bodies, at depths of a few kilometres, is in contrast with experimental evidence obtained by soil drilling at Campi Flegrei (Judenherc and Zollo, 2004), which excludes the presence of magma at shallow depths (≤ 2 km). In addition, many studies concerning the Campi Flegrei unrest episodes have established, in recent years, that it is important to consider the effects of hydrothermal fluid migration (e.g. Bonafede, 1990; Lima *et al*. 2009; D'Auria *et al*., 2014; Chiodini *et al*., 2015). Therefore, to model the ground displacement observed at the caldera of Campi Flegrei, the effects of its hydrothermal system (e.g. Todesco *et al*., 2014; Nespoli *et al*., 2021), superimposable to the ones of possible magmatic sources, cannot be neglected.

The thermo-poro-elastic (TPE) inclusion models represent the case where changes of pore pressure, Δp, and temperature, ΔT, occur within a volume of limited extent, filled with a porous

and permeable material (Fig. 2a). The changes in p and T produce deformation (and stress) in the surrounding medium (matrix), hence it is possible to refer to the TPE inclusion also in terms of deformation source. The matrix is assumed to be in isothermal and drained conditions [$\Delta p = 0$, $\Delta T = 0$; e.g. Wang (2001)]. Differently from pressurised cavity models, the TPE sources provide high deviatoric stress values within the source itself and can, therefore, justify the presence of earthquakes within them (e.g. Mantiloni *et al*., 2020). For example, at Campi Flegrei, the tomography of Calò and Tramelli (2018) suggests the existence of a rock layer with a thickness of about 500 m at a depth of about 2-3 km, likely placed above a deeper magmatic source (e.g. Nespoli *et al*., 2021; Buono *et al*., 2022) and below the shallow aquifer. Such a layer is subjected to changes in temperature and pore pressure due to the infiltration of the fluids released from the deeper magma reservoir (Fig. 2a). According to the geodetic data inversion performed by Nespoli *et al*. (2021), the deformation of the 1982-1984 unrest can be well reproduced employing a cylindrical TPE inclusion, located at a depth of about 2 km, with a radius of about 2.5 km and thickness of 500 m.

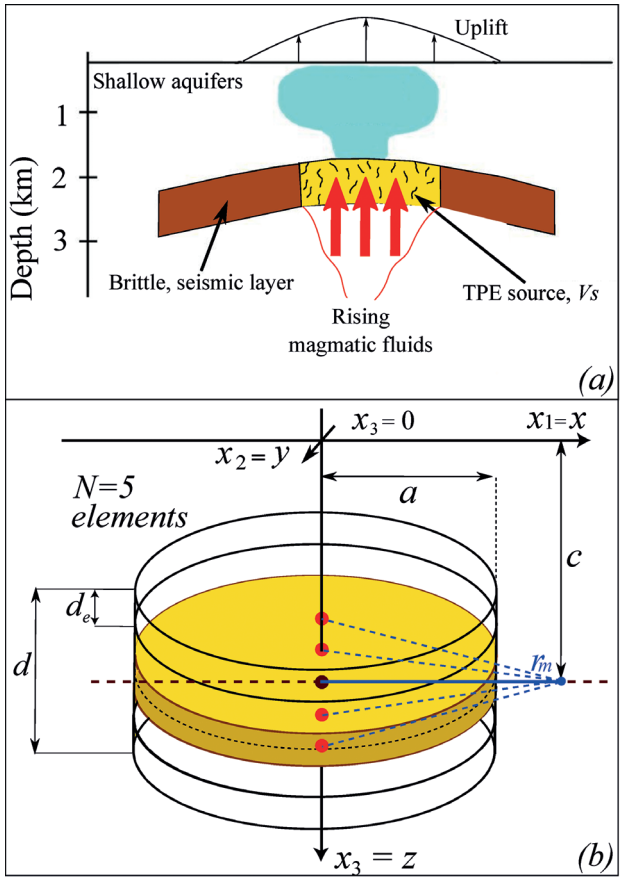

Fig. 2 - Representation of the hydrothermal system beneath the city of Pozzuoli (a). The magmatic fluids are released by a deep magma chamber; hot and pressurised fluids (red arrows) cross the rock layer through its permeable part (yellow). The fluids can, then, reach the surface through the shallow aquifers. Cylindrical TPE source model of thickness d and radius a embedded into a half-space (b). The TPE inclusion is modelled by superimposing N discs of equal thickness. Coordinate r is the distance of the field point (blue dotted lines) from the centre of each of the discs (red dots). Since for the same field point this distance depends on the disc, in panel b, $r = r_m$ is indicated as the distance of the field point from the centre of the m-th disc.

Recent literature proposes different approaches to model the mechanical effects of TPE inclusions. Some authors have used a numerical approach (e.g. Nespoli *et al*., 2021 and 2022), others analytical or semi-analytical approaches (Mantiloni *et al*., 2020; Belardinelli *et al*., 2022). While numerical methods allow for greater versatility in the geometrical representation of TPE inclusions, analytical methods are also very important, as they provide a starting point for more complex numerical models. In particular, each numerical model should be previously tested by comparing it with the analytical solutions available. One of the limitations of the analytical solutions, provided by Mantiloni *et al*. (2020) and Belardinelli *et al*. (2022), is that the geometry of the TPE inclusions is restricted to the case of a thin disc, i.e. with a thickness much smaller than its radius. This restriction may not be valid for all kinds of geophysical applications. However, Nespoli *et al*. (2021) proved that this limitation can be bypassed by representing a thick (cylindrical) TPE inclusion as a superposition (Fig. 2b) of thin TPE discs, as guaranteed by the unicity of the solution and continuity of the tractions over the TPE inclusion boundaries. It is, therefore, reasonable to assume that the greater the number of discs, the better the representation of the cylindrical TPE source model. However, to date there is still no study that addresses the problem in a quantitative way. Providing an answer to this problem may extend the applicability of the TPE sources.

For this reason, the aim of the present paper is to evaluate the minimum number of discs, N^*, suitable to model the displacement and stress field caused by a TPE cylindrical source with finite thickness, d, and radius, a. The inclusion is realised by overlapping disc-shaped TPE elements (discretised model) with the same radius and a thickness equal to a fraction of d.

The following paragraphs describe: the methodology used to calculate stress and displacement for the discretised model, and how to evaluate N^* and the maximum aspect ratio, d/a, that a TPE cylinder can have in order to be represented using only one element, also known as the 'disc solution'.

2. Methodology

2.1. Constitutive relationships for disc-shaped TPE inclusion in a half-space

To compute the displacement and stress fields generated by a TPE source, we started from the constitutive equation of a TPE medium expressing strain, ϵ_{ij}, as a function of stress, τ_{ij} (Biot, 1941; McTigue, 1986; Rice and Cleary, 1999). If a medium undergoing a temperature variation, ΔT, and a pore pressure variation, Δp, is considered, the following constitutive equation is obtained:

$$\epsilon_{ij} = \frac{1}{2\mu}\left(\tau_{ij} - \frac{\nu}{1+\nu}\tau_{kk}\delta_{ij}\right) + \epsilon_0\delta_{ij} \tag{1}$$

where:

$$\epsilon_0 = \frac{1}{3H}\Delta p + \frac{1}{3}\alpha\Delta T \tag{2}$$

and $K = \frac{2\mu(1+\nu)}{3(1-2\nu)}$ is the bulk modulus, $1/H$ is the poro-elastic expansion coefficient as defined by Biot (1941), μ is the medium rigidity, υ is the Poisson modulus, α is the thermal expansion coefficient.

A TPE region subjected to ΔT and Δp, confined within a closed volume V_s, defines a TPE inclusion, which can be modelled by generalising the method described by Eshelby (1957) and later, also, by Aki and Richards (1980). According to Belardinelli *et al*. (2019) a TPE inclusion located in a poro-elastic half-space, in drained and isothermal conditions, generates a displacement that can be expressed as follows:

$$u_i = 3K\epsilon_0 \int_{V_s} \frac{\partial G_{ik}}{\partial x'_k}(\boldsymbol{x}, \boldsymbol{x}'), dv(\boldsymbol{x}') \tag{3}$$

where ϵ_0, called 'TPE inclusion potency', is defined in Eq. 2 and G_{ik} is the Green's tensor for an elastic half-space. The latter enables evaluating displacement in the *i*-th direction at $\boldsymbol{x}$ (receiver point), generated by a unitary force acting in the *k*-th direction located at $\boldsymbol{x}'$ (source point). From the displacement field, the strain field can be computed as:

$$\epsilon_{ij} = \frac{1}{2}\left(\frac{\partial u_i}{\partial x_j} + \frac{\partial u_j}{\partial x_i}\right) \tag{4}$$

and the stress field (e.g. Mantiloni *et al*., 2020) as:

$$\tau_{ij}^{in} = 2\mu\epsilon_{ij} + \lambda\epsilon_{kk}\delta_{ij} - 3K\epsilon_0\delta_{ij} \quad \text{if the stress is calculated inside the source,} \tag{5}$$

$$\tau_{ij}^{out} = 2\mu\epsilon_{ij} + \lambda\epsilon_{kk}\delta_{ij} \quad \text{if the stress is calculated outside the source.} \tag{6}$$

In the case of a TPE disc with thickness *d* and radius *a*, the displacement (as well as the strain and stress) can be expressed as the sum of a non-singular part, $\mathbf{u}^{ns}$ (Mantiloni *et al*., 2020), and a singular part, $\mathbf{u}^{s}$ (Belardinelli *et al*., 2022), with the singularity being in $r = a$ (Fig. 2*b*):

$$u_i = u_i^s + u_i^{ns} \tag{7}$$

$$\epsilon_{ij} = \epsilon_{ij}^s + \epsilon_{ij}^{ns} \tag{8}$$

$$\tau_{ij}^{in} = 2\mu\left(\epsilon_{ij}^{ns} + \epsilon_{ij}^{s}\right) + \lambda(\epsilon_{kk}^{ns} + \epsilon_{kk}^{s})\delta_{ij} - 3K\epsilon_0\delta_{ij} \quad \text{if the stress is calculated inside the source} \tag{9}$$

$$\tau_{ij}^{out} = 2\mu\left(\epsilon_{ij}^{ns} + \epsilon_{ij}^{s}\right) + \lambda\epsilon_{kk}^{ns}\delta_{ij} \quad \text{if the stress is calculated outside the source.} \tag{10}$$

Here following, only the displacement component, $u_x = u_1$ and $u_z = u_3$, and the non-vanishing stress components, in $x_2 = 0$, $\tau_{xx} = \tau_{11}$, $\tau_{yy} = \tau_{22}$, $\tau_{zz} = \tau_{33}$, $\tau_{xz} = \tau_{13}$ (Mantiloni *et al.,* 2020), will be considered.

2.2. Discretised cylinder model

Assuming that the TPE source is a cylinder with a finite thickness, it can be discretised in thin discs, called elements, with thickness $d_e = d/N$ and aligned along the *z*-axis (Fig. 2b). In the

model, an odd number of discs will be considered since the central element is positioned along the median plane of the TPE source and centred in $z = c$. Next, the centre of the other elements is shifted by $m(d/N)$, where m represents the m-th disc above ($m > 0$) or below ($m < 0$) the central disc (numbered with $m = 0$).

Using Eqs. 7 to 10, it is possible to calculate the displacement and stress field of each of the cylinder elements under the assumption $d_e/a << 1$ and considering the centre of each disc to be at a depth of $c^{(m)} = c + m \cdot d_e$, $m = -(N-1)/2, \ldots, 0, \ldots, (N-1)/2$.

To reproduce the overall displacement and stress fields of the discretised cylinder, the contribution of each element is summed:

$$u_i = \sum_{m=-\frac{N-1}{2}}^{\frac{N-1}{2}} u_i^{(m)} \tag{11}$$

$$\tau_{ij} = \sum_{m=-\frac{N-1}{2}}^{\frac{N-1}{2}} \tau_{ij}^{(m)} \tag{12}$$

where $\tau_{ij}^{(m)}$ is:

$$\tau_{ij}^{(m)}(x,z) = \lambda \epsilon_{kk}^{(m)} \delta_{ij} + 2\mu \epsilon_{ij}^{(m)} - 3K\epsilon_o \delta_{ij} \quad if \quad |x| \le a, \left|z - c^{(m)}\right| < \frac{d_e}{2}, z > 0 \tag{13}$$

$$\tau_{ij}^{(m)}(x,z) = \lambda \epsilon_{kk}^{(m)} \delta_{ij} + 2\mu \epsilon_{ij}^{(m)} \qquad if \quad |x| \le a, \left|z - c^{(m)}\right| > \frac{d_e}{2}, z > 0 \tag{14}$$

$$\tau_{ij}^{(m)}(x,z) = \lambda \epsilon_{kk}^{(m)} \delta_{ij} + 2\mu \epsilon_{ij}^{(m)} \qquad if \quad |x| > a, z > 0\,. \tag{15}$$

2.3. Discretisation criteria depending on thickness

In this section, the criteria used to find the minimum number of elements, N^*, suitable to represent the displacement and stress fields for a cylindrical TPE inclusion, are discussed. To understand how well the disc solution of Mantiloni *et al.* (2020) can represent a TPE cylinder with finite thickness, the difference between a component of the displacement generated by a discretised model with N elements, $u^{(N)}$, and one with only one element, $u^{(1)}$, is estimated using the Root Mean Square Error, RMSE (e.g. Despotovic *et al*., 2016):

$$R_N(z) = \sqrt{\frac{1}{P}\sum_{k=1}^{P}[u^{(N)}(x_k,z) - u^{(1)}(x_k,z)]^2} \tag{16}$$

where displacements are evaluated at the point (x_k, z), and $P = 193$ represents the number of points considered on the x-axis in the interval $0 < x/a < 2$, with the cylinder axis being located in $x = 0$.

Assuming the existence of a minimum number of elements, N_u^*, such that the addition of further elements does not entail significant variations in the displacement field, the following discretisation criterion is used to denote N_u^*:

$$N_u^* = min(N) \text{ so that } |R_{N+2} - R_N| < \in_u. \quad (17)$$

For the present application, $\in_u = 7\times10^{-3}$ m is chosen, and this choice will be discussed in section 5. N_u* depends on depth of the field point, *z,* and on the displacement component. Ultimately, the maximum value obtained for N_u*(*z*) is chosen among all displacement components to represent the appropriate number of elements with which the displacement, due to a cylinder TPE source of thickness *d*, can be modelled.

Attention should be drawn to the fact that all points falling within the following range were intentionally excluded from the calculation of R_N:

$$0.96 < \frac{r}{a} < 1.04 \quad (18)$$

as the displacement field is singular in *r* = *a*. This arbitrary choice is made to limit the effect of the singularity on the estimate of N_u*. Besides this, within the interval in Eq. 18, the convergence requires caution in evaluating the singular part of displacement, as shown in Fig. A1 of Belardinelli *et al*. (2022).

Similarly, the equations to compute the RMSE for a stress component τ are:

$$S_N(z) = \sqrt{\frac{1}{P}\sum_{k=1}^{P}[\tau^{(N)}(x_k, z) - \tau^{(1)}(x_k, z)]^2} \quad (19)$$

and

$$N_s^* = min(N) \ \ so\ that\ |S_{N+2} - S_N| < \in_s \quad (20)$$

where $\in_s = 7\times10^{-4}$ Pa. Once more, the points within the interval given in Eq. 18 were excluded from the calculation of S_N as the stress components have a singularity in *r* = *a*. Eventually, N_s* was chosen as the maximum value of N_s*(*z*), among all stress components.

3. Study cases

The mechanical effects induced in two cases assuming different aspect ratios for the inclusions, were compared. In both cases, cylinders, with a centre located at a depth of *c* = 3000 m and radius of *a* = 500 m, were taken into consideration. In the first case (C1), a thickness of *d* = 50 m, with an aspect-ratio of *d*/*a* = 0.1, was assumed, while in the second case (C2), *d* = 500 m, with a greater aspect-ratio *d*/*a* = 1, was assumed. The effects of considering a different number of elements (*N* = 1 to 21), to discretise the inclusions of C1 and C2, were studied. On the median plane of the inclusion (Fig. 2b), the displacement component, u_1 was evaluated first of all.

For C1 (Fig. 3a), it can be seen that the differences, $\Delta u_1(N)$, between u_1, calculated with 1 element, and *N* elements increase in magnitude with *N*, but quickly reach an asymptotic value for *N* ≥ 5 and are quite low, $\Delta u_1 < 0.002$ m. In fact, when cylinder C1 is discretised with one, three, or five discs, a significant variation is obtained only at the cylinder edge, but moving both outwards and towards the source (*x* ≤ 0.95a and *x* ≥ 1.05a), the variations are negligible (Fig. 3b).

The vertical component of displacement, u_3, is not shown because the variations, $\Delta u_3(N)$, are in the order of $\Delta u_3 = 10^{-13}$ m, and can be neglected. The same is true for all the displacement components in $z = 0$ (surface level), where the disc solution is suitable for case C1. It should be noted that an inclusion is being modelled with the median plane located at a depth of $z = c = 3000$ m, which is greater than the cylinder thickness and radius; had a source at a shallower depth been considered, the effects of discretisation could have been more evident at the surface.

Fig. 3c shows the result obtained for C2. It is evident that the differences, $\Delta u_1(N)$, are greater than those of C1. In fact, Fig. 3c shows that $\Delta u_1(N) \sim 0.2$ m for $N > 1$, i.e. two orders of magnitude larger than the one obtained in C1. For C2, the single-element model considerably deviates from the discrete solutions (Fig. 3d). It can be observed that, for $N = 3$ and $N = 5$, the u_1 curves deviate from the one with $N = 1$ by a non-negligible difference ($\cong 0.1$ m) even at a relatively large distance from the boundary of the inclusion.

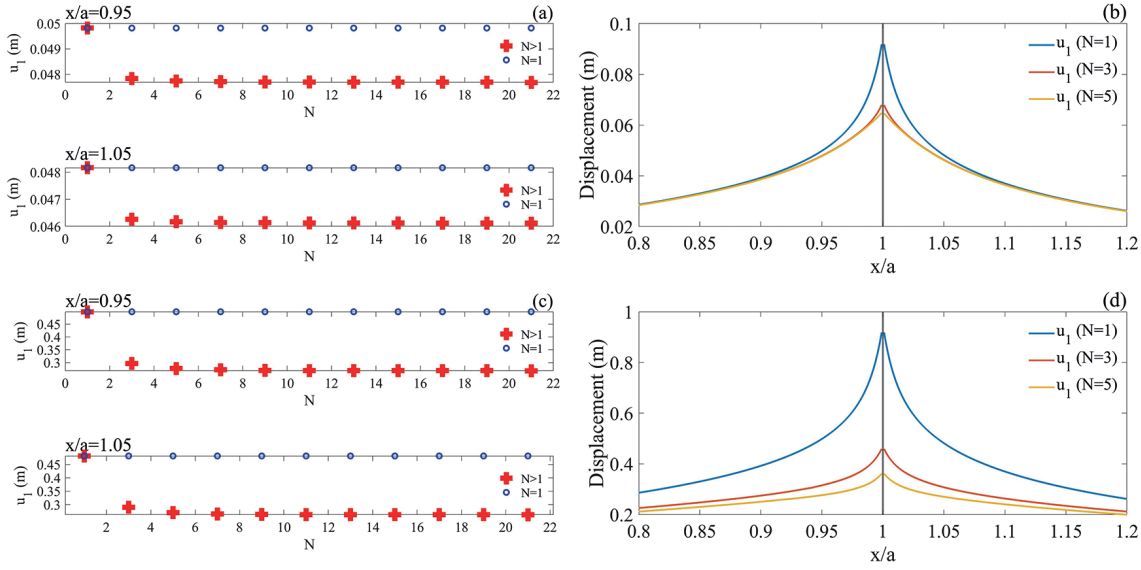

Fig. 3 - For a cylinder with $d = 50$ m: a) horizontal displacement represented as a function of N (number of elements) at points $x_{in}/a = 0.95$ (inside the source) and $x_{out}/a = 1.05$ (outside the source); b) horizontal component of displacement as a function of x/a in the cases $N = 1$, $N = 3$, and $N = 5$. For a cylinder with $d = 500$ m; c) horizontal displacement represented as a function of N (number of elements) at points $x_{in}/a = 0.95$ (inside the source) and $x_{out}/a = 1.05$ (outside the source); d) horizontal component of displacement as a function of x/a in the cases $N = 1$, $N = 3$, and $N = 5$. The median plane of the TPE cylinder is located at a depth of $z = c = 3000$ m.

At this stage, if how the value of stress components varies inside and outside the source as a function of the number of elements, N, is considered, then the difference between the $N = 1$ model and the $N = 3$ model for C1 is indicatively in the order of 10^6–10^5 Pa, and varies depending on the position (inside or outside the source) and on the stress components (Fig. 4a). Similarly to the displacement case, all the stress components almost reach an asymptotic value for $N > 3$. In Fig. 4c, the discretisation affects components τ_{11} and τ_{33}, with a maximum variation value of 10^7 Pa, which is close to the singularity at $x = a$; conversely, for τ_{22} the effect is much smaller. In Fig. 4b, the greatest variations obtained for C2 are encountered for τ_{11} and τ_{33} and are $\geq 5\times10^7$ Pa, while for τ_{22} they are less than 10^7 Pa.

As shown in Fig. 4d, for the C2 case, the components mostly affected by the discretisation are τ_{11} and τ_{33}, with a greater effect than in the C1 case.

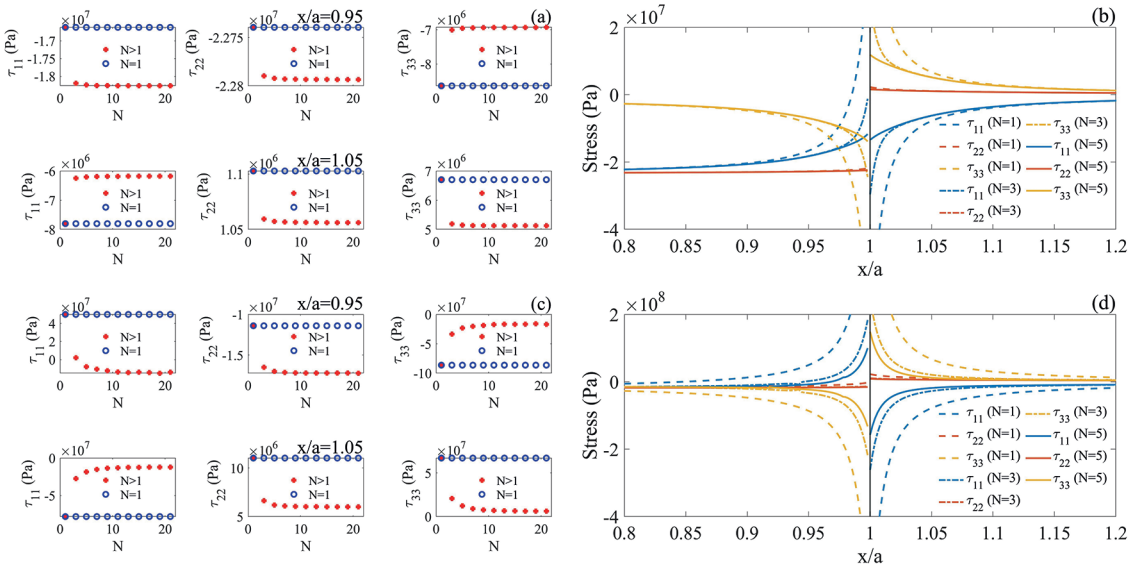

Fig. 4 - For a cylinder with d = 50 m: a) stress components represented as a function of N (number of elements) at points x_{in}/a = 0.95 (inside the source) and x_{out}/a = 1.05 (outside the source); b) stress components as a function of x/a in the cases N = 1, N = 3, and N = 5. For a cylinder with d = 500 m; c) stress components represented as a function of N (number of elements) at points x_{in}/a = 0.95 (inside the source) and x_{out}/a = 1.05 (outside the source); d) stress components as a function of x/a in the cases N = 1, N = 3, and N = 5. The median plane of the TPE cylinder is located at a depth of $z = c$ = 3000 m.

4. Error estimate using a disc solution

Starting from Eqs. 17 and 20 and the criteria established in the section 2, the study now focuses on how N_u* or N_S* vary as functions of the thickness, d. Figs. 3a and 3c suggest that N_u* corresponds to one element for C1 (d = 50 m), and three elements for C2 (d = 500 m), as quantitatively confirmed by results shown in Fig. 5a. In Figs 4a and 4c, particularly for stress components τ_{11} and τ_{33}, the asymptotic values are evidently reached at a greater N, with respect to u_1, which is confirmed by the greater N_S* values displayed in Fig. 5b. As shown in Figs. 5a and 5b, the discretisation criterion applied to the stress components (Eq. 20), in particular to τ_{33} and τ_{11}, is more restrictive than the one applied to the displacement and requires a larger number of elements, N_S*, for the same thickness.

Fig. 5c shows how R_N changes as a function of inclusion thickness. As mentioned above, the vertical component of the displacement provides no significant variation in the discretisation of the TPE cylinder and, as a matter of fact, the value calculated for N_u* is always equal to one element. For components τ_{33} and τ_{11} (up to 10^7 Pa for $d = a$ = 1), the RMSE, S_N, reaches considerably higher values compared to those obtained for component τ_{22} (10^6 Pa) (Fig. 5). This confirms that τ_{33} and τ_{11} are more affected by discretisation than τ_{22}, also in agreement with results shown in Fig. 4b.

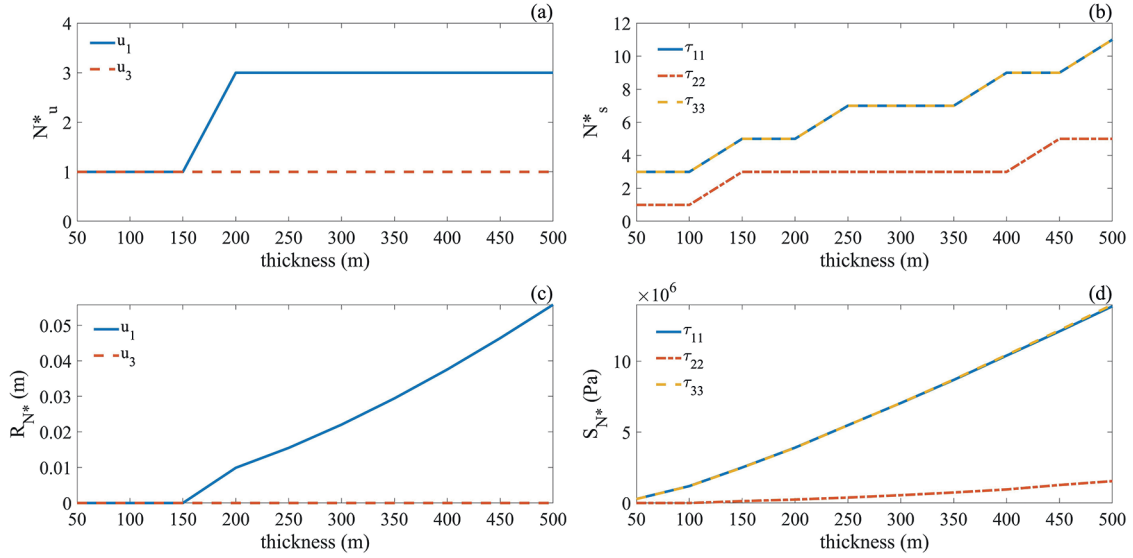

Fig. 5 - a) N_u* as a function of thickness (calculated with Eq. 17); b) N_s* as a function of thickness (calculated with Eq. 20); c) R_N as a function of thickness (calculated with N* = N_u*); d) S_N as a function of thickness (calculated with N* = N_s*). The median plane of the TPE cylinder is located at a depth of z = c = 3000 m.

Given a certain thickness, N* was ultimately chosen as the maximum between N_s* and N_u*, which consistently is N_s*, according to results shown in Figs. 5a and 5b.

Therefore, wanting to represent both displacement and stresses with a precision that is higher than a given threshold ($\in_U$ = 7×10^{-3} m, and $\in_S$ = 7×10^4 Pa, respectively, for this application), it is necessary to discretise the cylindrical source of thickness, d, with the number of elements reported in Table 1.

Considering the values obtained in Table 1, the number of elements required is extremely low for lower aspect ratios, being N* = 3 for d/a < 0.3, and rises as the thickness-radius ratio increases.

From the values in Table 1, the element thickness, d_e, that must be used to discretise a cylinder of thickness d (d_e = d/N), can be evaluated according to the criterion in Eq. 20. Therefore, it is possible to state that the thickness of the discretising elements ranges between 16 and 50 m (hence $d_e/a \leq 0.1$).

N*was found to increase with an increasing d, and, therefore, the errors made by representing a cylindrical TPE source with a disc solution are also expected to increase at an increasing source thickness. Consistently, R_{N^*} and S_{N^*} (the RMSE functions for displacements and stresses on the median plane) increased with an increasing d (cf. Figs. 5c and 5d).

Since both displacement and stress scales with d (cf., e.g. Figs. 3b and 3d or Figs. 4b and 4d), it may now be advisable to introduce an estimator that evaluates the relative error due to a particular choice of discretisation. The average relative error associated with a displacement component, u, at the (x, z) coordinate point, evaluated using a disc model $u^{(1)}$ instead of the N*-element model $u^{(N)}$, can be evaluated as the Root Mean Square Relative Error, RMSRE (e.g. Despotovic *et al.*, 2016):

$$\frac{\Delta u}{u}(z) = \sqrt{\frac{1}{P}\sum_{k=1}^{P}\frac{\left[u^{(N^*)}(x_k,z)-u^{(1)}(x_k,z)\right]^2}{\left[u^{(N^*)}(x_k,z)\right]^2}} \quad (21)$$

Table 1 - Number N^* of elements obtained for τ_{33} (Fig. 5b) as a function of thickness.

Aspect ratio, d/a	Total inclusion thickness, d (m)	Number of elements, N^*	d_e(m)
0.1	50	3	16.7
0.2	100	3	33.3
0.3	150	5	30
0.4	200	5	40
0.5	250	7	35.7
0.6	300	7	42.9
0.7	350	7	50
0.8	400	9	44.4
0.9	450	9	50
1	500	11	45.5

where x_k is a point along the horizontal profile at constant z.

Similarly, the RMSRE associated with a stress component evaluated using a disc model $\tau^{(1)}$, instead of the N^*-element model $\tau^{(N^*)}$, is:

$$\frac{\Delta\tau}{\tau}(z) = \sqrt{\frac{1}{P}\sum_{k=1}^{P}\frac{\left[\tau^{(N^*)}(x_k,z)-\tau^{(1)}(x_k,z)\right]^2}{\left[\tau^{(N^*)}(x_k,z)\right]^2}} \quad . \tag{22}$$

In both Eqs. 21 and 22, N^* represents the maximum value obtained between N_u^* and N_S^*.

In the calculation of the RMSRE, a ring around the cylinder edge is excluded, and it is the same ring as the one indicated in the count of R_N and S_N, to avoid accounting for errors associated with the values of stress and displacement close to a singularity.

The results obtained for different values of d are shown in Fig. 6a, for displacement, and in Fig. 6b, for stress and summarised in Table 2. The RMSRE increases at the increasing of disc thickness, and is smaller for displacement than for stress.

The maximum thickness, d_{MAX}, below which the single disc model is considered acceptable, is defined according to the maximum RMSRE value tolerable in this study. A RMSRE significantly greater than 30% indicates poor model results (e.g. Podowitz *et al.*, 2014; Torres and Fuertes, 2021). For instance, if we consider the RMSRE relative to τ_{33} computed on the median plane of the cylinder, we obtain a RMSRE of 31% for d_{MAX} = 150 m (cf. Fig. 6b and Table 2), which corresponds to an aspect ratio of d/a = 0.3. Therefore, such value is considered as the maximum acceptable aspect ratio for a single element model. The fact that the threshold value, d_{MAX}, depends on the error required by the problem being studied must be taken into consideration: the smaller the error, the greater the need to discretise cylinders with ever smaller thicknesses.

As a further example, the C2 cylinder source, with a thickness of d = 500 m (d/a = 1), is taken into consideration: in Figs. 6c and 6d, the displacement and diagonal stress component obtained are shown on the median plane with a single disc model (dashed lines) and a discretised cylinder with N^* = 11 (solid lines). The average error introduced by the disc model is in the order of 0.5 cm for the horizontal displacement, and about 1 MPa for stress components τ_{11} and τ_{33}.

Table 2 - Maximum RMSRE(%) committed when using the disc model in place of the discretised model of a cylindrical TPE inclusion as a function of thickness. The RMSRE is evaluated for the component in the median plane of the inclusion.

Aspect ratio, *d*/*a*	Total inclusion thickness, *d* (m)	RMSRE (%)
0.1	50	5
0.2	100	16
0.3	150	31
0.4	200	45
0.5	250	63
0.6	300	80
0.7	350	96
0.8	400	120
0.9	450	140
1	500	166

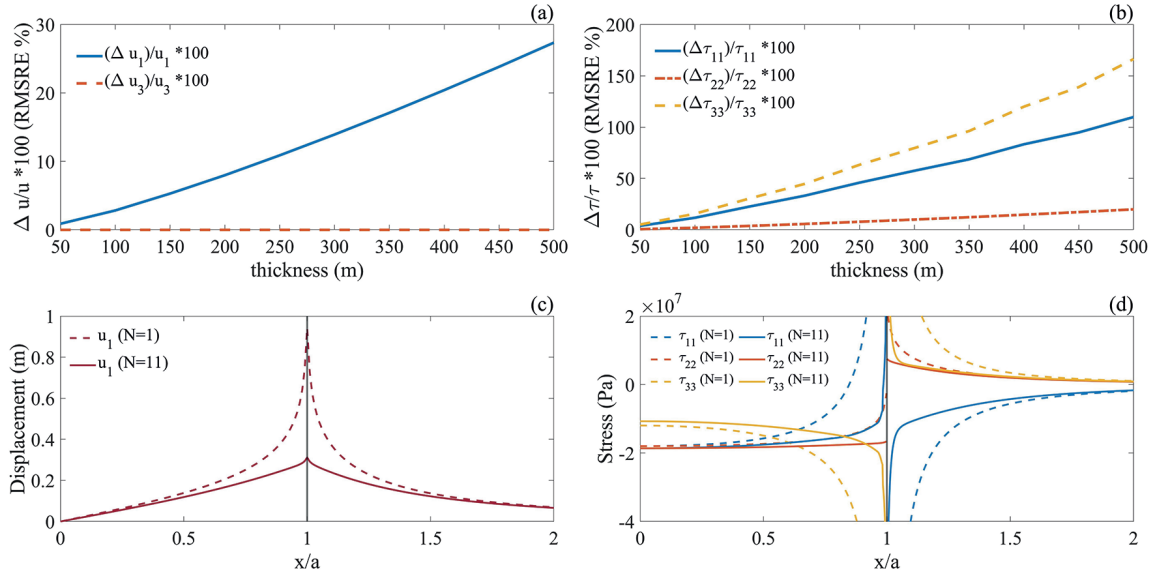

Fig. 6 - Percentage error (RMSRE) for displacement, computed with Eq. 21 (a), and for stress, computed with Eq. 22 (b). Using $N = 1$ and $N = N^* = 11$, comparison of displacement (c) and stress (d) for a cylinder of thickness $d = 500$ m. The median plane of the TPE cylinder is located at a depth of $z = c = 3000$ m.

5. Discussion

By comparing the mechanical responses of two TPE cylinders located at the same depth, with different aspect ratios, assuming the same radius, $a = 500$ m, and two different thicknesses of 50 and 500 m (Figs. 3 and 4), the greatest difference between the effects generated by the single disc and discretised cylinder are obtained in the median plane of the source, for stress component τ_{33}. For each thickness, *d,* the minimum number of elements, N^*, beyond which R_N and S_N reached a stable value lower than $\in_S = 7\times10^{-3}$ m, for displacement, and $\in_S = 7\times10^{4}$ Pa, for stress, was

calculated. Such values were chosen considering that the current precision of InSAR is around 1 cm and that the vertical component from GPS systems is provided within some millimetres of uncertainty, while the modelled stresses in the median plane of the TPE source (Figs. 4c, 4d, 5c, 5d) are considerably greater than 10^5 Pa. To be certain that displacement and stress components were evaluated within a precision of at least 1 cm and 0.1 MPa, respectively, we chose $\in_U$ and $\in_S$ to be 30% lower than these values (e.g. with $\in_S = 10^4$ Pa it would be necessary to use $N_S = 15$ elements to represent a cylinder of thickness $d = 500$ m).

The results indicate that the N_S* number depends on the stress component considered. In particular, normal stress on horizontal surfaces, τ_{33}, is the component most affected by discretisation and requires the maximum number of elements N_S*. The maximum thickness, d_e, of the elements used to discretise a cylinder is between 16 and 50 m. Accordingly, elements should have aspect ratios smaller than 0.1, where the thickness is one order of magnitude smaller than the radius.

This study has also shown that, by using a single disk model, the relative errors on the median plane, with respect to a discretised model with $N = N^*$, are consistently below ~30%, for aspect ratios lower than 0.3. If, for example, the unrest episode of the Campi Flegrei area dated 1982-1984 and the geometry of the TPE inclusions used by Mantiloni *et al*. (2020), with an aspect ratio of d/a in the range from 0.1 to 0.3, are considered, the displacement field in the median plane is found to be not significantly affected by discretisation. *A fortiori*, as seen at the beginning of section 3, this also applies to the displacement computed at the surface. This result is important as it confirms that a single disc TPE model is suitable for geodetic data inversion, and a single disc model makes the inversion process much faster.

One of the major limitations of our approach is related to the singularities appearing near $r = r_m = a$ for the m-th disc element (Fig. 2b). In the worst case faced in this work, a discretised cylinder with $d = a$ and a field point located in the median plane ($z = c$), from geometrical considerations, the singularities of all the elements sum up within the interval $0.87 < x/a \leq 1$. To bypass the problem within this interval, the truncation order in the expansion of the singular components can be increased and/or the solution of each element near the singularities (Belardinelli *et al*., 2022) interpolated, as done in this work. To evaluate the displacement and stress field in any point inside a thicker TPE cylinder ($d > a$), the use of a numerical approach is convenient (Nespoli *et al*., 2022).

As rather deep TPE inclusions have been considered so far (i.e. located at a depth greater than their radius), the results obtained indicate that the discretisation does not significantly affect the fields computed on the surface. In the case of shallow TPE inclusions (depth smaller than radius a, but larger than thickness d), surface fields would be affected by the singularities appearing near $r = r_m = a$ and attention should be paid to model them even at $z = 0$.

The mechanical effects induced by a TPE inclusion are much larger on the inside than on the outside, reaching the maximum on the median plane of the cylinder (e.g. Mantiloni *et al*., 2020; Nespoli *et al*., 2021; Belardinelli *et al*., 2022). For this reason, the choice of a suitable number of elements to represent a thick TPE inclusion should be made considering the mechanical effects computed on the median plane of the cylinder. This condition is also valid in the case of shallow TPE inclusions ($d < c < a$).

6. Conclusions

In the present paper, the mechanical responses of two cylindrical TPE inclusions with different aspect ratios (thickness over radius) are compared, and the error made in representing

the two inclusions with the single disc solution evaluated. In addition, the minimum number of disc elements, suitable to represent both inclusions with a given precision, is determined. Identifying this number is important in order to ensure that a model is sufficiently accurate to be compared with the geophysical observables (e.g. surface displacement), but also to avoid using an excessively large number of elements that would lead to an unnecessary increase in the calculation time, especially in non-linear inversion processes. This would also increase computational problems arising from the singularities of the analytical solutions, occurring at $r = a$, for each element. Our results show that, for an aspect ratio lower or equal to 0.3, a single element model is suitable to represent both displacement and stress, with a sufficient accuracy. A higher aspect ratio would lead to an RMSRE significantly greater than 30% in the estimation of the stress field in the median plane. Accordingly, the geometry of the TPE source inferred by Mantiloni *et al*. (2020) to model the surface displacement in the 1982-1984 Campi Flegrei unrest, having d/a = 0.3, falls within the acceptable range.

Conversely, to represent an inclusion with an aspect ratio equal to one, considering 11 elements would be the optimal solution. The results obtained in this work also indicate that the greatest differences, between the effects generated by the disc solution and the thick discretised model, are obtained in the median plane of the inclusion, for stress component. The approach used to discretise TPE inclusions could also be applied when these sources are in a viscoelastic (VE) half-space [TPVE inclusions: Nespoli *et al*. (2023)]. The results obtained are also important in representing the transient effect of vertical fluid propagation inside a TPE when the inclusion potency varies with time and depth (e.g. Belardinelli *et al*., 2022). For these reasons, we think that the results of the present work are worthy of consideration for the proper use of TPE deformation source models.

Acknowledgments. This paper is based on the results presented at the GNGTS 2023 conference as: "The hot topic of thermo-poro-elastic deformation sources in volcanic and geothermal fields" by M. Nespoli, M.E. Belardinelli, and M. Bonafede. We thank the editor Dario Slejko, an anonymous reviewer and Francesco Maccaferri for their useful comments, which significantly improved the manuscript. Matlab scripts, representing a disc-shaped TPE inclusion embedded in a viscoelastic half-space, are available from Nespoli *et al.* (2023), and can be downloaded from https://github.com/Massimones/TPVE_solutions.git. The scripts are also accessible via Zenodo (https://doi.org/10.5281/zenodo.7898877).

REFERENCES

Aki K. and Richards P.; 1980: *Quantitative Seismology: theory and methods, vol. 1.* W.H. Freeman and Company, San Francisco, CA, USA, 557 pp.

Belardinelli M.E., Bizzarri A., Berrino G. and Ricciardi G.P.; 2011: *A model for seismicity rates observed during the 1982-1984 unrest at Campi Flegrei caldera (Italy)*. Earth Planet. Sci. Lett., 302, 287-298, doi: 10.1016/j.epsl.2010.12.015.

Belardinelli M.E., Bonafede M. and Nespoli M.; 2019: *Stress heterogeneities and failure mechanism induced by temperature and pore pressure increase in volcanic regions.* Earth Planet. Sci. Lett., 525, 115765, 24 pp., doi: 10.1016/j.epsl.2019.115765.

Belardinelli M.E., Nespoli M. and Bonafede M.; 2022: *Stress changes caused by exsolution of magmatic fluids within an axisymmetric inclusion*. Geophys. J. Int., 230, 870-892, doi: 10.1093/gji/ggac093.

Biot M.A.; 1941: *General theory of three-dimensional consolidation.* J. Appl. Phys., 12, 155-164.

Bonafede M.; 1990: *Axi-symmetric deformation of a thermos-poro-elastic half space: inflation of a magma chamber.* Geophys. J. Int., 103, 289-299.

Bonafede M., Amoruso A., Crescentini L., Gottsmann J.H., Todesco M. and Trasatti E.; 2022: *Source modelling from ground deformation and gravity changes at the Campi Flegrei caldera, Italy*. In: Orsi G., D'Antonio M. and Civetta L. (eds), Campi Flegrei, Active volcanoes of the World, Springer Verlag, Berlin, Heidelberg, Germany, pp. 283-309, doi: 10.1007/978-3-642-37060-1_11.

Buono G., Paonita A., Pappalardo L., Caliro S., Tramelli A. and Chiodini G.; 2022: *New insights into the recent magma dynamics under Campi Flegrei caldera (Italy) from petrological and geochemical evidence.* J. Geophys. Res.: Solid Earth, 127, e2021JB023773, 15 pp., doi: 10.1029/2021JB023773.

Calò M. and Tramelli A.; 2018: *Anatomy of the Campi Flegrei caldera using Enhanced Seismic Tomography Models*. Sci. Rep., 8, 16254, 12 pp., doi: 10.1038/s41598-018-34456-x

Chiodini G., Vandemeulebrouck J., Caliro S., D'Auria L., Martino P., Mangia-Capra A. and Petrillo Z.; 2015: *Evidence of thermal-driven processes triggering the 2005-2014 unrest at Campi Flegrei caldera*. Earth Planet. Sci. Lett., 414, 58-67.

Chiodini G., Caliro S., Avino R., Bini G., Giudicepietro F., De Cesare W., Ricciolino P., Aiuppa A., Cardellini C., Petrillo Z., Selva J., Siniscalchi A. and Tripaldi S.; 2021: *Hydrothermal pressure-temperature control on CO_2 emissions and seismicity at Campi Flegrei (Italy)*. Journal of Volcanology and Geothermal Research, 414, 10 pp., doi: 10.1016/j.jvolgeores.2021.107245.

D'Auria, Giudicepietro F., Aquino I., Borriello G., Del Gaudio C., Lo Bascio D., Martini M., Ricciardi G.P., Ricciolino P. and Ricco C.; 2014: *Repeated fluid-transfer episodes as a mechanism for the recent dynamics of Campi Flegrei caldera (1989-2010).* J. Geophys. Res.: Solid Earth, 116, B04313, 24 pp., doi: 10.1029/2010JB007837.

De Martino P., Dolce M., Brandi G., Scarpato G. and Tammaro U.; 2021: *The ground deformation history of the Neapolitan volcanic area (Campi Flegrei caldera, Somma-Vesuvius volcano, and Ischia Island) from 20 years of continuous GPS observations (2000-2019)*. Remote Sens., 13, 2725, 18 pp., doi: 10.3390/rs13142725.

De Vivo B., Belkin H.E. and Rolandi G. (eds); 2020: *Introduction to Vesuvius, Campi Flegrei and Campanian volcanism.* Elsevier Inc., Amsterdam, The Netherlands, pp. 1-8, doi: 10.1016/B978-0-12-816454-9.00001-8.

Del Gaudio C., Aquino I., Ricciardi G.P., Ricco C. and Scandone R.; 2010: *Unrest episodes at Campi Flegrei: a reconstruction of vertical ground movements during 1905-2009.* J. Volcanol. Geotherm. Res., 195, 48-56, doi: 10.1016/j.jvolgeores.2010.05.014.

Despotovic M., Nedic V., Despotovic D. and Cvetanovic S.; 2016: *Evaluation of empirical models for predicting monthly mean horizontal diffuse solar radiation.* Renewable Sustainable Energy Rev., 56, 246-260, doi: 10.1016/j.rser.2015.11.058.

Eshelby J.D.; 1957: *The determination of the elastic field of an ellipsoidal inclusion, and related problems.* Proc. R. Soc. London, Ser. A., 241, 376-396, doi: 10.1098/rspa.1957.0133.

Fialko Y., Khazan Y. and Simons M.; 2001: *Deformation due to a pressurised horizontal circular crack in an elastic half-space, with applications of volcano geodesy.* Geophys. J. Int., 144, 300-308.

Judenherc S. and Zollo A.; 2004: *The bay of Naples (southern Italy): constraints on the volcanic structures inferred from a dense seismic survey.* J. Geophys. Res.: Solid Earth, 109, B10312, 10 pp., doi: 10.1029/2003JB002876.

Lima A., De Vivo B., Spera F.J., Bodnar R.J., Mila A., Nunziata C., Belking H.E. and Cannatelli C.; 2009: *Thermodynamic model for uplift and deflation episodes (bradysism) associated with magmatic-hydrothermal activity at the Campi Flegrei (Italy)*. Earth-Sci. Rev., 97, 44-58, doi: 10.1016/j.earscirev.2009.10.001.

Mantiloni L., Belardinelli M.E., Bonafede M. and Nespoli M.; 2020: *Deformation and stress in hydrothermal regions: the case of a disk-shaped inclusion in a half space.* J. Volcanol. Geotherm. Res., 403, 107011, 28 pp., doi: 10.1016/j.jvolgeores.2020.107011.

McTigue D.F.; 1986: *Thermoelastic response of fluid saturated porous rock.* J. Geophys. Res.: Solid Earth, 91, 9533-9542, doi: 10.1029/JB091iB09p09533.

Mogi K.; 1958: *Relations between the eruption of various volcanoes and the deformation of the ground surface around them.* Res. Earthquake Inst., 36, 99-134.

Nespoli M., Belardinelli M.E. and Bonafede M.; 2021: *Stress and deformation induced in layered media by cylindrical thermo-poro-elastic sources: an application to Campi Flegrei (italy)*. J. Volcanol. Geotherm. Res., 415, 107269, 30 pp., doi: 10.1016/j.jvolgeores.2021.107269.

Nespoli M., Belardinelli M.E., Calò M., Tramelli A. and Bonafede M.; 2022: *Deformation induced by distributions of single forces in a layered half-space: EFGRN/EFCMP*. Comput. Geosci., 164, 105136, 32 pp., doi: 10.1016/j.cageo.2022.105136.

Nespoli M., Belardinelli M.E. and Bonafede M.; 2023: *Thermo-poro-viscoelastic response of a disc-shaped inclusion*. Geophys. J. Int., 235, 135-149, doi: 10.1093/gji/ggad212.

Podowitz D.I., Liu C., Yang P. and Yurkin M.A.; 2014: *Comparison of the pseudo-spectral time domain method and the discrete dipole approximation for light scattering by ice spheres*. J. Quant. Spectrosc. Radiat. Transfer, 146, 402-409, doi: 10.1016/j.jqsrt.2014.02.032.

Rice J.R. and Cleary M.P.; 1999: *Some basic stress diffusion solution for fluid-saturated elastic porous media with compressible constituents.* Rev. Geophys. Space Phys., 14, 227-241, doi: 10.1029/RG014i002p00227.

Todesco M., Costa A., Comastri A., Colleoni F., Spada G. and Quareni F.; 2014: *Vertical ground displacement at Campi Flegrei (Italy) in the fifth century: rapid subsidence driven by pore pressure drop.* Geophys. Res. Lett., 41, 1471-1478.

Torres B. and Fuertes D.; 2021: *Characterization of aerosol size properties from measurements of spectral optical depth: a global validation of the GRASP-AOD code using long-term AERONET data.* Atmos. Meas. Tech., 14, 4471-4506, doi: 10.5194/amt-14-4471-2021.

Trasatti E., Bonafede M., Ferrari C., Giunchi C. and Berrino G.; 2011: *On deformation sources in volcanic areas: modelling the Campi Flegrei (Italy) 1982-84 unrest.* Earth Planet. Sci. Lett., 306, 36 pp., doi: 10.1016/j.epsl.2011.03.033.

Troise C., Natale G.D., Schiavone R., Somma R. and Moretti R.; 2018: *The Campi Flegrei caldera unrest: discriminating magma intrusions from hydrothermal effects and implications for possible evolution.* Earth Sci. Rev., 188, 108-122.

Wang H.F.; 2001: *Theory of linear poroelasticity with applications to geomechanics and hydrogeology*. Princeton University Press, Princeton, NJ, USA, 304 pp., doi: 10.1515/9781400885688.

Yang X.M., Davis P.M. and Dieterich J.H.; 1988: *Deformation from inflation of a dipping finite prolate spheroid in an elastic half-space as a model for volcanic stressing.* J. Geophys. Res.: Solid Earth, 93, 4249-4257.

Corresponding author: Carolina Benussi
Department of Physics and Astronomy Augusto Righi, Alma Mater Studiorum, University of Bologna
Viale Berti Pichat 6/2, 40128 Bologna, Italy
Phone: +39 051 2095018; e-mail: carolina.benussi@studio.unibo.it